Supplementary Materials for

Sustainable lignin-hydroxymethyl furfural-based waterborne polyurethane adhesive with high bonding strength, water and weather resistance

Ying-An Mai[a], Xitai Cai[a], Libo Li[a], Zhipeng Qiu[,a], Weifeng Liu[*,a,b], Xueqing Qiu[c], Rongxian Ou[d], Jingpeng Zhou[b], Fengshan Zhang[b], Fan Bu[b]*

[a]– School of Chemistry and Chemical Engineering, State Key Laboratory of Advanced Papermaking and Paper-based Materials, Guangdong Provincial Key Lab of Green Chemical Product Technology, South China University of Technology, Wushan Road 381, Guangzhou 510640, P. R. China.

[b]– Shandong Huatai Paper Co., Ltd. Dongying 257337, China.

[c]– School of Chemical Engineering and Light Industry, Guangdong University of Technology, Waihuan Xi Road 100, Guangzhou, Guangdong, 510006, China.

[d]– Institute of Biomass Engineering, South China Agricultural University, Guangzhou, 510642, China

* Corresponding author. Tel.: +86 02087114722, E-mail: solorway@scut.edu.cn; weifengliu@scut.edu.cn.

Experimental Section

Characterize（All samples were vacuum-dried at 50 ℃ for 12 h before characterizations.）

Two-dimensional heteronuclear single quantum coherence NMR spectra (2D-HSQC) and phosphorus-31 NMR (^{31}P NMR) spectra were recorded on AVANCE III HD 600 MHz (Bruker, Germany). For the 2D-HSQC analysis, approximately 30 mg of lignin was dissolved in 0.6 mL of DMSO-d6. For ^{31}P-NMR analysis, a mixed solvent (solvent A) was prepared by combining deuterated pyridine and chloroform (1.6:1 ratio). An internal standard solution was made by dissolving 0.018 g of *N*-hydroxy-5-norbornene-2,3dicarboximide and 0.005 g of chromium (III) 2,4-pentanedionate relaxant in 1 mL of solvent A. After mixing 30 mg of lignin and 0.1 mL of the internal standard solution with 0.5 mL of solvent A the sample were stirred for 12 hours. Subsequently0.15 mL of 2-chloro-4,4,5,5-tetramethyl-1,3,2-dioxaphospholane was added. ^{31}P-NMR was conducted at room temperature with a 90^{o} pulse angle,25 s pulse interval, 250 signal numbers, and a scan width of 61.9 ppm.

Lap shear strength tests were conducted using beech wood substrates. Prior to bonding, the wood surfaces were not sanded, and the grain direction was oriented parallel to the long edge of the specimens. Unless otherwise stated, all bonding procedures were carried out at an ambient temperature of 23 ± 3 °C and a relative humidity of 30 ± 10%. The adhesive was applied to both bonding surfaces in two successive coatings, with an amount of 0.03 g per coating. A time interval of 10 min was allowed between the two coatings. After the second coating, the specimens were assembled after an additional 10 min. The assembled joints were then stored under closed conditions for 7 days at (23 ± 2) °C and 50 ± 10% relative humidity. Hot pressing was performed at pressures ranging from 1 to 2 MPa, with temperatures of 140 or 170 °C and pressing times of 5 or 10 min, as specified in the text. After hot pressing, the bonded

specimens were cooled to room temperature by forced air (fan cooling) and stored for an additional 24 h prior to mechanical testing.

WFP was estimated from the fractured surfaces after lap shear testing by evaluating the fraction of wood substrate failure within the bonded overlap area (visual inspection and image analysis).

Simulation Details

To model the wood surface, a cellulose Iβ surface was constructed using the Cellulose-builder program[1], which effectively captures the key structural features of cellulose microfibrils commonly found in higher plants such as wood[2, 3]. The cellulose surface model consists of 8 layers, each containing 6 cellulose chains, with 5 cellobiose units per chain. Additionally, α-Fe_2O_3(001) surfaces were constructed to study their interfacial interactions with the modified adhesives. These metal oxides were chosen as representative oxidized surfaces, as pure metals are readily passivated by the spontaneous formation of native oxide layers under ambient conditions[4]. The selected facets are widely recognized as thermodynamically stable surfaces for the respective oxides[5, 6], and are frequently used in interfacial simulations[7-11]. The crystal structure files were obtained from Krishan Kanhaiya et al.[7], where the structures were fully optimized.

In addition to the surfaces, three types of polymer chains—Blank, LWPU, and LHWPU—were constructed based on experimental formulations (Table S2). For simplicity, only the primary components were considered when constructing the models. Specifically, each Blank PU chain consists of 24 PPC units and 2 IPDI units, connected via DMPA, following the molar ratios used in the experimental synthesis. The LWPU and LHWPU chains were derived by incorporating lignin fragments into the Blank PU chain. For LWPU, AOH lignin was introduced, modeled using a monomeric composition of S: G: H = 7:2:1, as determined experimentally (Table S6). The lignin structure includes characteristic inter-unit linkages found

in native lignin, such as β-O-4, β–β, β–5, and 4-O-5, which represent typical C–O and C–C bonding motifs in lignocellulosic biomass[12]. For LHWPU, HMF molecules were further coupled into AOH lignin to construct HAOH. The incorporation of AOH and HAOH into the PU chains allows for a direct comparison of their interfacial interactions in subsequent simulations. Both the inorganic surfaces and PU chains were modeled using the INTERFACE force field (IFF)[7, 13] , which has been parameterized to accurately reproduce experimental interfacial interactions of metals, metal oxides, and polymers.

All molecular dynamics (MD) simulations in this work were performed using the Large-Scale Atomic/Molecular Massively Parallel Simulator (LAMMPS) package[14]. Periodic boundary conditions (PBC) were implemented in all directions. The Verlet-velocity integration algorithm with a timestep of 1.0 fs was used to integrate the equations of motion. Van der Waals interactions were calculated with a cutoff of 14.0 Å , with tail corrections, and long-range Coulomb interactions were computed using the Particle-Particle Particle-Mesh (PPPM) solver[15]. Temperature and pressure were controlled at 298.15 K and 1 atm using the Nose-Hoover thermostat[16]. Visualization and analysis of simulation results were performed using OVITO[17] and MD Analysis[18, 19]. A typical MD simulation was carried out in the NPT ensemble for 10 ns, with the last 5 ns used to analyze the interactions between the surfaces and PU chains, as shown in Figures 8a, 8b, and 8d. After full equilibration, during which the PU chains adhered firmly to the surfaces, deformation simulations were performed to evaluate their adhesive strength. The simulation box was elongated along the peeling direction at a constant engineering strain rate of $5 \times 106\ s^{-1}$. The engineering stress–strain curves were derived from the normal stress component in the loading direct

Sample	Lignin(g)	HMF(g)	NaOH(g)
AKL-HMF	5.00	2.95	0.24
AOH-HMF	5.00	4.06	0.36
DAOH-HMF	5.00	7.69	0.30

Table S1. Lignin-HMF formulation table with different lignin process

Table S2. LHWPU formulation table with different AOH-HMF content process

Sample	PPC (g)	Lignin-HMF/ Lignin (g)	DMPA (g)	IPDI (g)	DBTDL (g)	TEA (g)	Total Mass (g)	Lignin-HMF/Lignin content (%)
Blank	10.0	0	0.70	2.73	0.042	0.68	14.15	0
L-20	8.0	2.0	0.76	3.81	0.045	0.57	14.57	15.91
LH-10	9.0	1.0	0.73	3.27	0.043	0.55	14.59	6.85
LH-20	8.0	2.0	0.76	3.84	0.045	0.57	15.22	13.14
LH-30	7.0	3.0	0.79	4.39	0.047	0.60	15.83	18.95
LH-40	6.0	4.0	1.16	5.49	0.052	0.88	17.82	22.41
LH-50	5.0	5.0	1.21	6.05	0.053	0.91	18.22	27.44
LH-60	4.0	6.0	1.25	6.59	0.055	0.94	18.80	31.91
LH-70	3.0	7.0	1.29	7.13	0.057	0.97	19.45	35.99
LH-80	2.0	8.0	1.33	7.67	0.059	1.00	20.06	39.88

Table S3. Content of Various Hydroxyl Groups of AOH and DAOH

Chemical shift	Assignment	AOH (mmol/g)	DAOH (mmol/g)
~150-145.5	Aliphatic OH	1.38	0.07
~144.5-137.6	Phenolic OH	3.22	6.10
~144.5-140.2	C_5 substituted	2.70	2.77
~143.2-142.5	Syringyl	1.51	1.07
~140.2-138.5	Guaiacyl	0.49	1.62
~138.5-137.6	*P*-hydroxyphenyl	0.03	1.20
~136-133.6	Carboxylic acid	0.29	0.17
Total OH		4.60	6.17

Sample	Gel rate（%）
AKL-HMF	19.78
AOH-HMF	26.17
DAOH-HMF	88.06

Table S4. Gel rate of Lignin-HMF

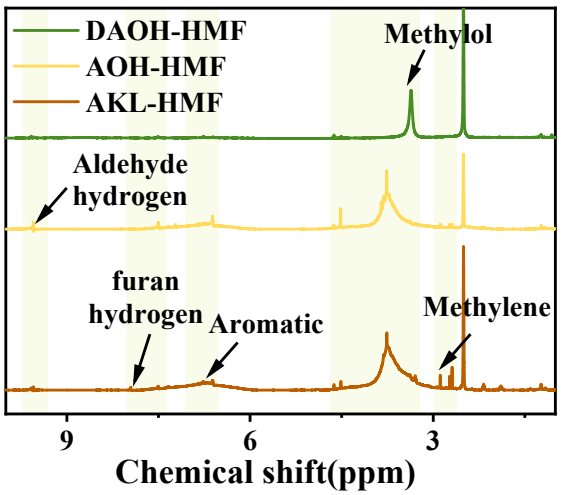

Figure S1. ^{1}H NMR spectra of Lignin-HMF

Table S5. T $_{5、10、20、max}$ and residue of AKL、AOH and Lignin-HMF

Sample	%Degradation			Temperature of maximum degradation(℃)	Residue(%)
	5	10	20		
AKL	226.50	266.22	318.79	342.56	50.13
AOH	207.36	284.18	334.13	358.23	43.95
AKL-HMF	240.36	290.01	347.32	369.52	47.38
AOH-HMF	259.04	307.57	353.72	372.53	48.88
DAOH-HMF	275.47	384.20	427.70	394.60	65.20

Table S6. Emulsion stability and particle size

Samples	Stability	D_{50} (nm)	PDI	Zeta potential (mV)
Blank	stable	59.78	0.12	76.93
LH-10	stable	59.59	0.17	86.47
LH-20	stable	60.05	0.25	69.91
LH-30	stable	73.58	0.10	65.23
LH-40	stable	84.48	0.19	54.61
LH-50	stable	129.8	0.13	58.16
LH-60	stable	124	0.20	57.96
LH-70	stable	142.2	0.24	58.95
LH-80	stable	124.6	0.20	52.47

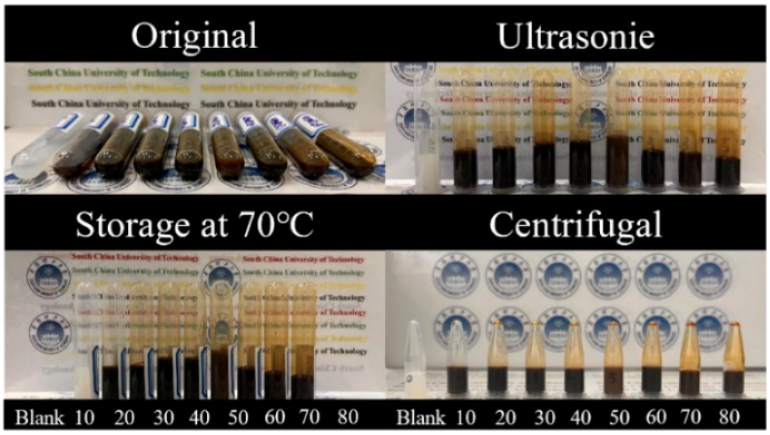

Figure S2. Storage stability of emulsion

Table S7. Composition ratio of polymers synthesized from different raw materials.

	M_w/M_n	Blank	LWPU	LHWPU
PPC	2000	24	24	24
IPDI	222.32	4	4	4
DMPA	134.13	2	2	2
AOH	809	0	6	0
AOH-HMF	1208	0	0	6
TEA	101.19	2	2	2
Total M_w		49359.92	54213.92	56607.92

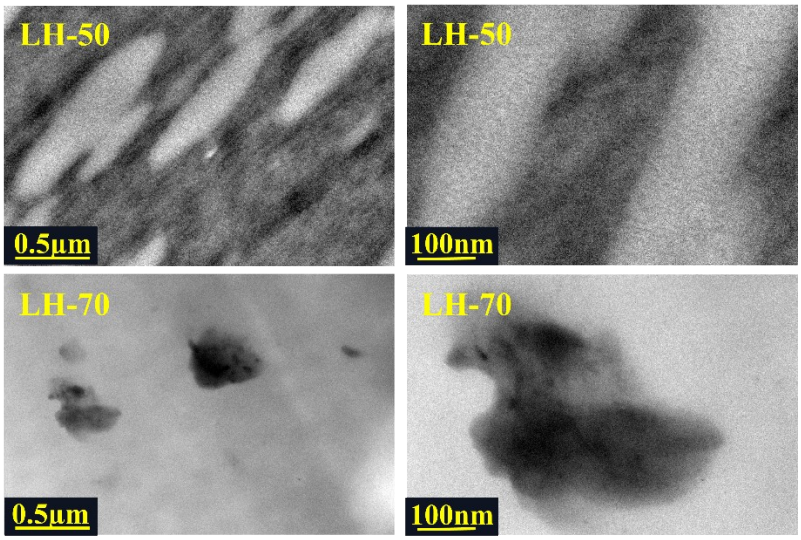

Figure S3. TEM images of LHWPU

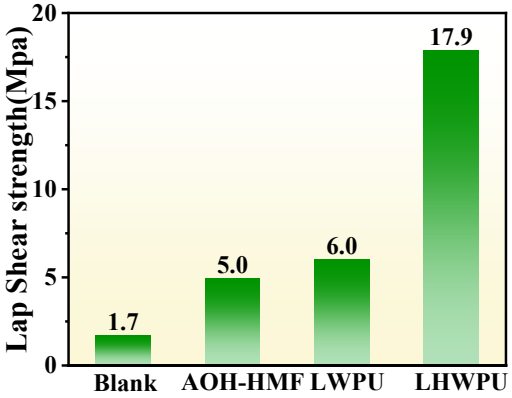

Figure S4. Lap Shear strength of Blank、AOH-HMF、LWPU and LHWPU on wood

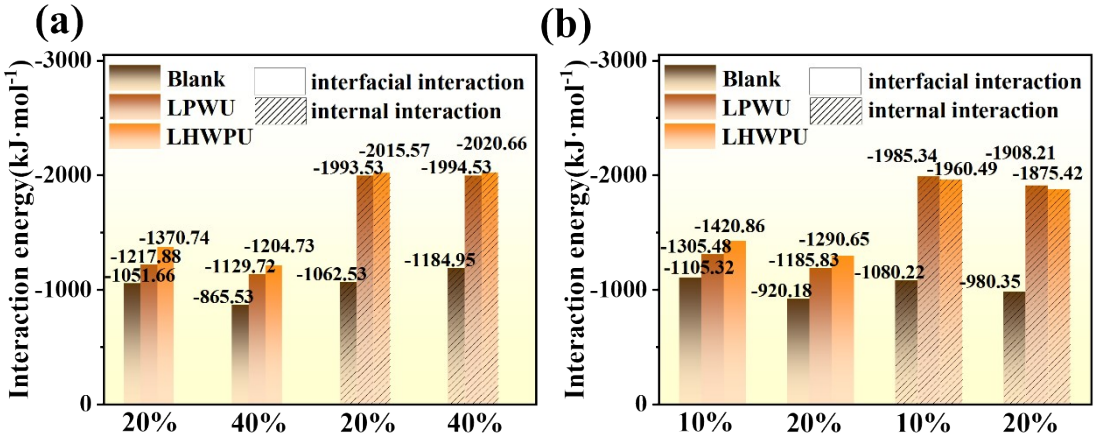

Figure S5. Interaction energies under different interfacial conditions: (a) surface hydroxyl density and (b) interfacial water content. For the surface hydroxyl density case, 20% and 40% of the surface hydroxyl groups on the substrate were selectively excluded from interacting with the PUs. For the interfacial water content case, water molecules corresponding to 10% and 20% water contents were inserted into the interfacial region. The water content is defined as water content (%)=mass of water/mass of surface.

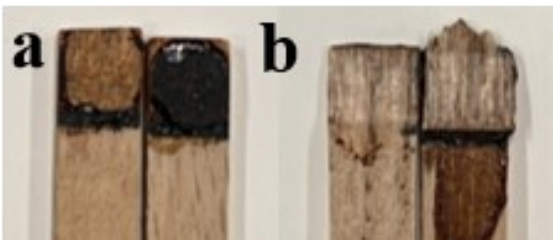

Figure S6. Images after lap shear test before (a) and after (b) hot pressing (LH-20)

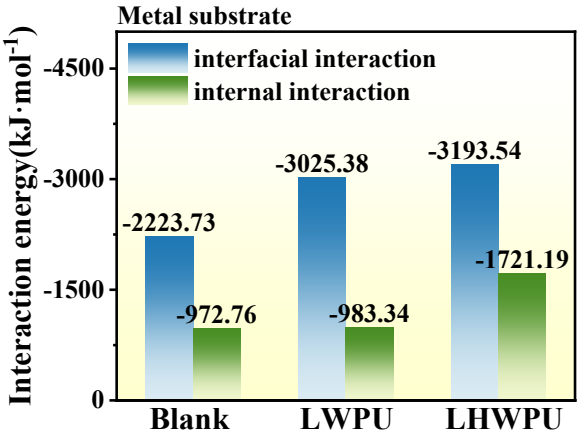

Figure S7. The interaction energy between metal and adhesive and between adhesive and adhesive

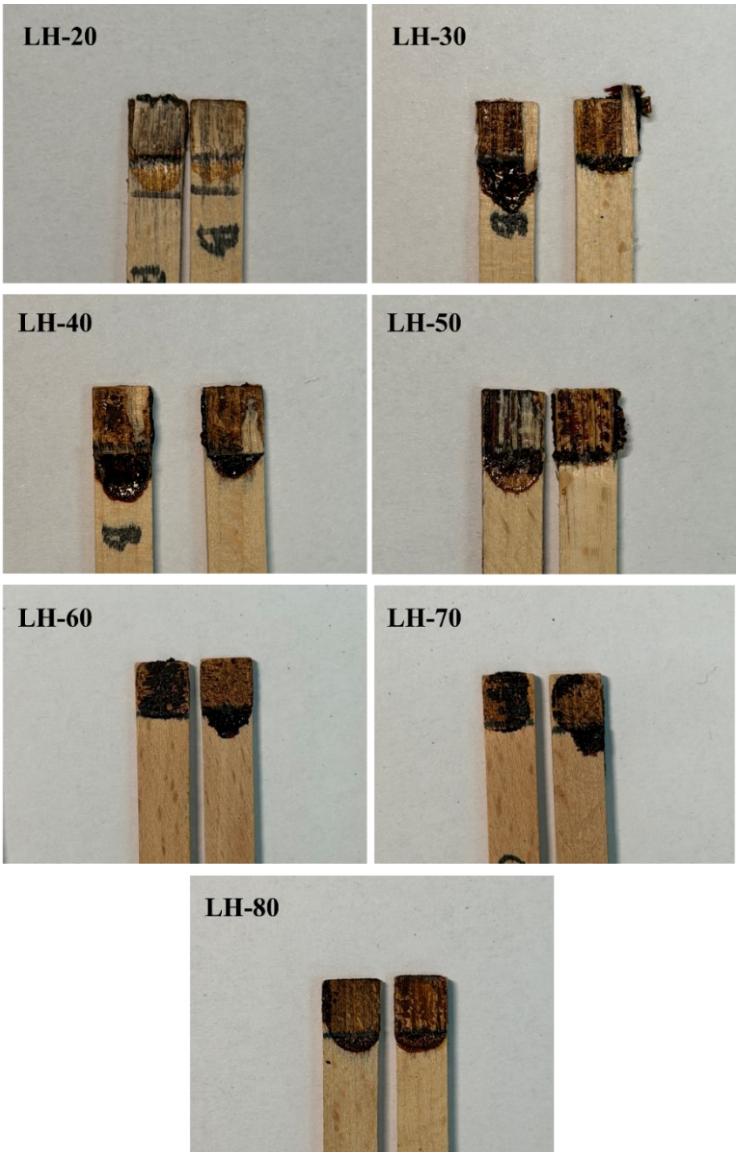

Figure S8. Adhesive surface images after lap shear test for sample LH-20~80

Table S8. WFP of LH-20~80

Sample	WFP(%)
LH-20	≈100
LH-30	40
LH-40	20
LH-50	20
LH-60	0
LH-70	0
LH-80	0

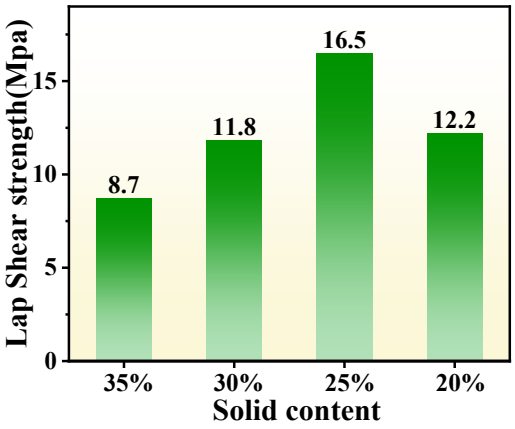

Figure S9. Lap Shear strength of LH-50 on beech wood under different solid contents.

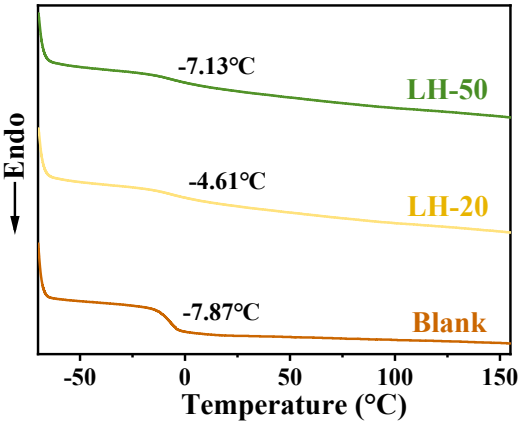

Figure S10. The DSC curve of LHWPU

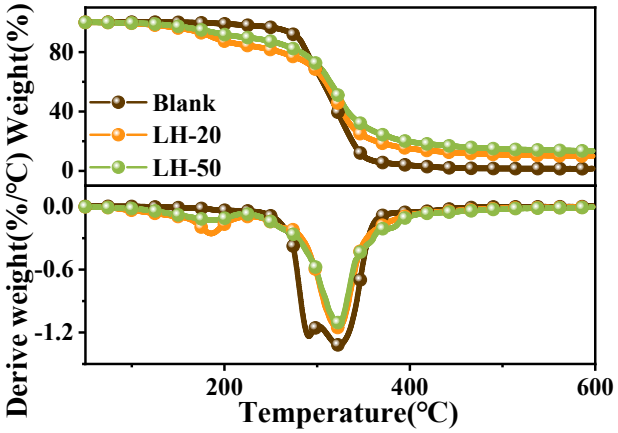

Figure S11. TG of LHWPU

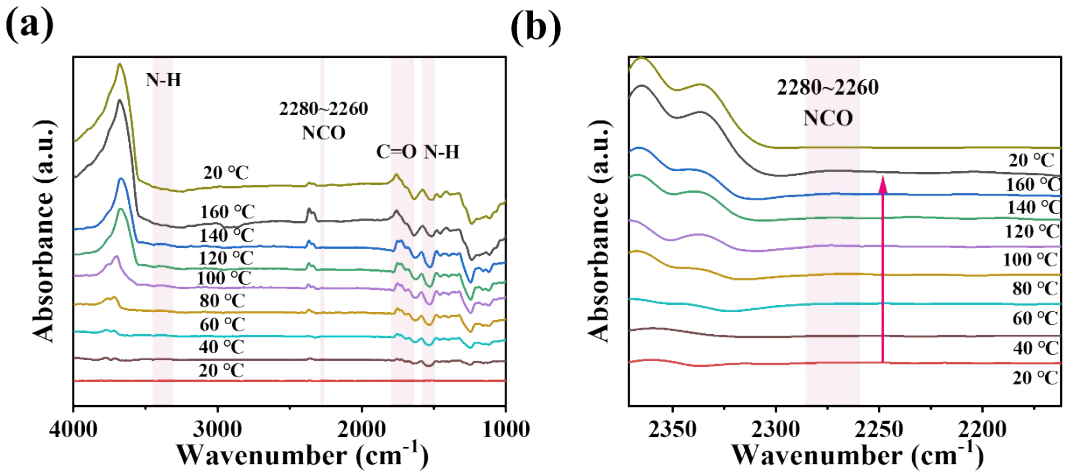

Figure S12. (a) ATR-FTIR spectra of the cured LHWPU film at different temperatures. (b) Enlarged ATR-FTIR spectra of the cured LHWPU film in the NCO stretching region (2280–2260 cm^{-1}) at different temperatures. The NCO band gradually emerges upon heating and disappears upon cooling back to 20 °C, indicating a reversible thermal dissociation and reformation of carbamate linkages.

Sample	%Degradation			Temperature of maximum degradation (°C)	Residue(%)
	15	30	50		
Blank	286.38	289.39	310.45	312.83	0.90
LH-20	225.56	297.66	315.72	316.72	10.24
LH-50	263.93	307.44	325.50	326.50	13.36

Table S9. $T_{15、30、50、max}$(℃) and residue of Blank、LH-20 and LH-50

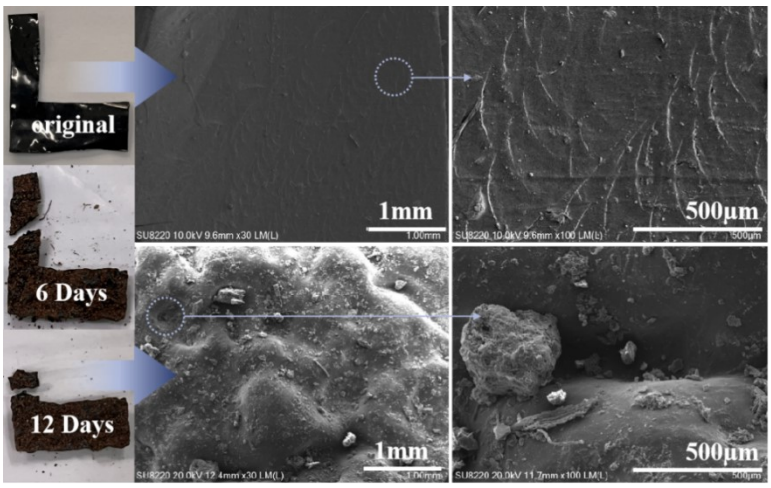

Figure S13. The pictures and SEM images of DAOH-HMF degradation in soil.

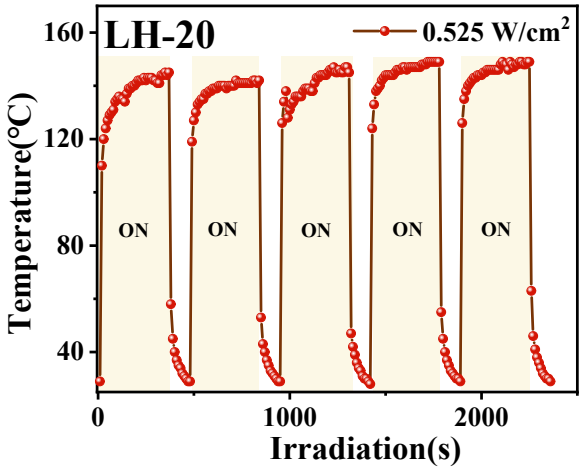

Figure S14. The photothermal temperature rising-cooling cycles of LH-20 at 0.525 W/cm^2.

Screening Carbon Footprint Assessment (CFP): A laboratory-scale screening carbon footprint assessment was conducted to evaluate the relative environmental contributions of process electricity and organic solvent use/recovery for representative adhesive systems. The assessment follows the general principles of ISO 14067 and is intended for hotspot identification at the laboratory scale.[20, 21]

Goal and scope: Functional unit: 1 kg of final adhesive product (LH-50: waterborne polyurethane latex; DAOH–HMF: aqueous resin); System boundary: laboratory gate-to-gate, including process electricity (heating, stirring, vacuum, rotary evaporation) and key solvent use/recovery; upstream raw material production and equipment manufacture were excluded; Electricity emission factor: 0.5777 kg $CO_2e \cdot kWh^{-1}$ (China 2024 average); Solvent recovery assumption: a conservative recovery rate of 25% was assumed for all recoverable organic solvents; the remaining fraction was treated as loss.

System 1: LH-50

Table S10. Composition of LH-50 (scaled to 1 kg adhesive)

Component	Mass (g)
AOH–HMF	82.3
PPC	82.3
DMPA	19.9
IPDI	99.6
DBTDL	0.87

Table S11. Electricity inventory for LH-50 preparation

Process step	Power (kW)	Time (h)	Electricity (kWh)
Heating (110–90 °C, multi-step)	0.50	11.0	5.50
Vacuum operation	0.37	2.0	0.74
Mechanical stirring	0.05	12.0	0.60
Acetone recovery (rotary evaporation)	1.50	0.17	0.25
Total per batch			**7.09**

Batch product mass: 0.0607 kg; Electricity per kg adhesive: 116.7 $kWh \cdot kg^{-1}$; Carbon footprint: 67.4 kg $CO_2e \cdot kg^{-1}$.

Table S12. Solvent use and recovery for LH-50

Solvent	Amount used	Recovery method	Recovery rate	Treated as loss
Acetone	10 mL	Rotary evaporation	25%	7.5 mL
NMP	2 mL	—	Not recovered	2 mL

System 2: DAOH–HMF aqueous resin

Table S13. Composition of DAOH–HMF resin (laboratory batch)

Component	Mass (g)
DAOH	5.00
HMF	7.69
NaOH	0.30
Water	23.38
Total	**36.37**

Table S14. Electricity inventory for DAOH–HMF resin synthesis (90 °C)

Process step	Power (kW)	Time (h)	Electricity (kWh)
Heating (90 °C)	**0.50**	**3.33**	**1.67**
Mechanical stirring	**0.50**	**3.33**	**0.17**
Total per batch			**1.83**

Table S15. Electricity inventory for DAOH preparation and solvent recovery

Process step	Power (kW)	Time (h)	Electricity (kWh)
Heating (150 °C, 12 h)	0.50	12.0	6.00
Mechanical stirring	0.05	12.0	0.60
DMF recovery (30 mL)	1.50	0.50	0.75
ICH recovery (12 mL)	1.50	0.25	0.38
Total per batch			**7.73**

Table S16. Summary of screening CFP results

Solvent / reagent	Amount used	Recovery method	Recovery rate
DMF	30ml	Vacuum distillation	25%
Iodocyclohexane	12ml	Vacuum distillation	25%
n-Hexane	15ml	Extraction	Not recovered

Table S17. Composition of LH-50 (scaled to 1 kg adhesive)

System	Electricity ($kWh \cdot kg^{-1}$)	Carbon footprint ($kg\ CO_2e \cdot kg^{-1}$)	Dominant hotspot
LH-50	116.7	67.4	Heating & vacuum
DAOH–HMF resin	409.7	236.6	High-temperature activation

These results demonstrate that, at laboratory scale, process electricity dominates the carbon footprint, while solvent-related impacts can be effectively reduced through recovery and recycling. The absolute values are inflated by small batch sizes and are therefore not intended as industrial benchmarks, but rather as indicators for process optimization and sustainability improvement.

References

1. T. C. Gomes and M. S. Skaf, *J Comput Chem*, 2012, **33**, 1338-1346.
2. Y. Nishiyama, P. Langan and H. Chanzy, *Journal of the American Chemical Society*, 2002, **124**, 9074-9082.
3. T. Imai and J. Sugiyama, *Macromolecules*, 1998, **31**, 6275-6279.
4. V. E. Henrich, *Reports on Progress in Physics*, 1985, **48**, 1481.
5. G. S. Parkinson, *Surface Science Reports*, 2016, **71**, 272-365.
6. Z. Liu, L. Ma and A. S. M. Junaid, *The Journal of Physical Chemistry C*, 2010, **114**, 4445-4450.
7. K. Kanhaiya, M. Nathanson, P. J. in ’t Veld, C. Zhu, I. Nikiforov, E. B. Tadmor, Y. K. Choi, W. Im, R. K. Mishra and H. Heinz, *Journal of Chemical Theory and Computation*, 2023, **19**, 8293-8322.
8. T. Semoto, Y. Tsuji and K. Yoshizawa, *The Journal of Physical Chemistry C*, 2011, **115**, 11701-11708.
9. M. T. Ajide and N. J. English, *The Journal of Physical Chemistry C*, 2023, **127**, 24088-24105.
10. F. R. Negreiros, L. S. Pedroza and G. M. Dalpian, *The Journal of Physical Chemistry C*, 2016, **120**, 11918-11925.
11. T. Saito, E. Shoji, M. Kubo, T. Tsukada, G. Kikugawa and D. Surblys, *The Journal of Chemical Physics*, 2021, **154**, 114703.
12. L. Shuai, M. T. Amiri, Y. M. Questell-Santiago, F. Héroguel, Y. Li, H. Kim, R. Meilan, C. Chapple, J. Ralph and J. S. Luterbacher, *Science*, 2016, **354**, 329-333.
13. H. Heinz, T.-J. Lin, R. Kishore Mishra and F. S. Emami, *Langmuir*, 2013, **29**, 1754-1765.
14. A. P. Thompson, H. M. Aktulga, R. Berger, D. S. Bolintineanu, W. M. Brown, P. S. Crozier, P. J. in 't Veld, A. Kohlmeyer, S. G. Moore, T. D. Nguyen, R. Shan, M. J. Stevens, J. Tranchida, C. Trott and S. J. Plimpton, *Computer Physics Communications*, 2022, **271**, 108171.
15. R. W. Hockney and J. W. Eastwood, *Computer simulation using particles*, CRC Press, 1988.
16. S. Nosé, *The Journal of Chemical Physics*, 1984, **81**, 511-519.
17. A. Stukowski, *Modell. Simul. Mater. Sci. Eng.*, 2009, **18**, 015012.
18. N. Michaud-Agrawal, E. J. Denning, T. B. Woolf and O. Beckstein, *J Comput Chem*, 2011, **32**, 2319-2327.
19. R. Gowers, M. Linke, J. Barnoud, T. Reddy, M. Melo, S. L. Seyler, J. Domański, D. Dotson, S. Buchoux, I. Kenney and O. Beckstein, in *Proceedings of the 15th Python inScience Conference*, eds. S. Benthall and S. Rostrup, SciPy, 2016, DOI: https://doi.org/10.25080/Majora-629e541a-00e, pp. 98-105.
20. G. Wernet, C. Bauer, B. Steubing, J. Reinhard, E. Moreno-Ruiz and B. Weidema, *The International Journal of Life Cycle Assessment*, 2016, **21**, 1218-1230.
21. T. Dandres, N. Vandromme, G. Obrekht, A. Wong, K. K. Nguyen, Y. Lemieux, M. Cheriet and R. Samson, *Journal of Industrial Ecology*, 2017, **21**, 1312-1322.